PAPER

Polarization and Spatial Statistics of Wideband MIMO Relay Channels in Urban Environment at 2.35 GHz

Xin NIE[†a)], ***Student Member***, **Jianhua ZHANG**[††], ***and*** **Ping ZHANG**[†], ***Members***

SUMMARY Relay, which promises to enhance the performance of future communication networks, is one of the most promising techniques for IMT-Advanced systems. In this paper, multiple-input multiple-output (MIMO) relay channels based on outdoor measurements are investigated. We focus on the link between the base station (BS) and the relay station (RS) as well as the link between the RS and the mobile station (MS). First of all, the channels were measured employing a real-time channel sounder in IMT-Advanced frequency band (2.35 GHz with 50 MHz bandwidth). Then, the parameters of multipath components (MPCs) are extracted utilizing space-alternating generalized expectation algorithm. MPC parameters of the two links are statistically analyzed and compared. The polarization and spatial statistics are gotten. The trends of power azimuth spectrum (PAS) and cross-polarization discrimination (XPD) with the separation between the RS and the MS are investigated. Based on the PAS, the propagation mechanisms of line-of-sight and non-line-of-sight scenarios are analyzed. Furthermore, an approximate closed-form expression of channel correlation is derived. The impacts of PAS and XPD on the channel correlation are studied. Finally, some guidelines for the antenna configurations of the BS, the RS and the MS are presented. The results reveal the different characteristics of relay channels and provide the basis for the practical deployment of relay systems.

key words: *MIMO relay channels, wideband outdoor measurements, cross-polarization discrimination, power azimuth spectrum, channel correlation*

1. Introduction

Recently, the relay-based communication system has been attracting great attention because of its various advantages over conventional cellular systems regarding the enhancement of diversity, achievable rates and coverage [1], [2]. Relay-based multi-input multi-output (MIMO) system typically comprises the base station (BS), the relay station (RS), and the mobile station (MS), each equipped with multiple antennas. The RS forwards the data received wirelessly from the BS to the MS, and vice versa. Accordingly, the relay channel consists of three individual links, i.e., the link between the BS and the RS (BS-RS link), the link between the RS and the MS (RS-MS link), as well as the link between the BS and the MS (BS-MS link). In a typical application scenario, there is LOS existing between the BS and the RS to maximize the coverage [3]. The height of relay antennas is lower than that of BS antennas in order to reduce operating and maintenance costs [2].

Most theoretical works on relay-based systems have been carried out under simplified assumption for the channel properties. For example, the Rayleigh channel, which no longer applies when the line-of-sight (LOS) exists, is widely used for analysis [4], [5]. As a result, the deviation of the actual performance from theoretical performance is still of great significance. More details of the relay channels need to be included in the channel model to narrow the gap. Although the most effective and straightforward way to obtain the channel characteristics is to conduct channel measurements, former researches mainly focus on the measurement and modeling of the conventional BS-MS link. For an overview of state-of-the-art channel measurements and models, see [6]–[8] and the references therein. The reduction in RS antenna height gives rise to changes in scattering environments. The results measured from the BS-MS link are not suitable for the BS-RS and RS-MS links. Current researches related to relay channel measurements lay emphasis on the validation of relay performance, i.e., data rate and bit error ratio (BER). In [9], [10], the channel impulse responses (CIRs) of indoor relay channels were measured and rate improvements of different relay schemes were assessed based on CIRs. The effect of relay location on channel capacity was reported in [11]. The achievable date rate of relay system in real outdoor-to-indoor scenario was predicted in [12], [13]. In [14], a real-time DSP-based testbed was constructed and BERs of cooperating relaying schemes were tested. Due to the limitation of experimental facilities, the propagation statistics of relay channels were not discussed in these works. Besides, the measurement results of wideband outdoor relay channel are scarce. Moreover, the relay measurements conducted in IMT-Advance frequency bands were not reported in the previous works.

In order to obtain a more thorough understanding of the fundamental properties of relay channels, we conducted a measurement campaign at the center frequency of 2.35 GHz with 50 MHz bandwidth. As mentioned above, the height of RS antennas is lower than that of BS antennas. The different properties of BS-RS and RS-MS links are of our main concern. The channel correlation greatly impacts on the relay performance [15]. Polarization diversity and spatial diversity are two main approaches to reduce the channel correlation and to enhance the diversity/multiplexing gain

Manuscript received August 27, 2009.
Manuscript revised May 24, 2010.

[†]The authors are with the Key Laboratory of Universal Wireless Communications, Ministry of Education, Beijing University of Posts and Telecommunications, P.O. box 92, No. 10 XiTu Cheng Road, Haidian District, Beijing 100876, China.

[††]The author is with the Wireless Technology Innovation Institute, Beijing University of Posts and Telecommunications, P.O. box 92, No. 10 XiTu Cheng Road, Haidian District, Beijing 100876, China.

a) E-mail: niexin1983@gmail.com

DOI: 10.1587/transcom.E94.B.139

[16], [17]. The polarization diversity is mainly determined by the cross-polarization discrimination (XPD) [18], while the spatial diversity is primarily decided by the power azimuth spectrum (PAS) [19]. The impacts of antenna height on the polarization and spatial statistics were not considered in previous channel models, , which means that the parameters for describing the spatial and polarization statistics of the channel are regarded as independent on the antenna height. Thus, we lay our emphasis on the polarization and spatial statistics. The main contributions of this paper are: a) we present the polarization and spatial statistics of BS-RS and RS-MS links; b) we analyze the distribution of XPDs in vertical and horizontal polarization and the dependence of XPDs on distance; c) we propose a multi-cluster Laplacian distribution to model the PAS, and study the dominating propagation mechanisms in LOS and non-line-of-sight (NLOS) scenarios; and d) we derive a closed-form approximation to investigate the impacts of both XPDs and PAS on the channel correlation. The results and analysis given here are informative to provide guidelines for antenna configurations and the deployment of relay-based systems.

The rest of this paper is organized as follows. Section 2 describes the measurement equipments and environment. Section 3 shows the procedure of data post-processing. Section 4 presents polarization and spatial statistics of measured relay channels, mainly including XPD, PAS, and channel correlation. The propagation mechanisms in LOS and NLOS scenarios are also analyzed. Section 5 gives the conclusion of our work.

2. Measurements

2.1 Equipment

The Elektrobit PropSound Channel Sounder was employed, which is described in more detail in [20]. The sounder worked in a time-division multiplexing mode. Periodic pseudo random binary signals (PRBS) were transmitted between different Tx-Rx antenna pairs. The interval within which all antenna pairs are sounded once is referred to as a *measurement cycle*. The omnidirectional array (ODA), which consists of 28 dual-polarized elements, was employed at the BS, the RS and the MS. Every element of the ODA consists of two co-located feeds, the polarization directions of which are +45° and −45° with respect to the vertical, respectively. The spacing between the neighboring elements is half a wavelength. The ODA used in measurements is shown in Fig. 1. The resolution of parameter estimation is determined by the number of antennas [21]. A large number of antennas are required in the measurement to obtain accurate estimation. Thus, one ring of the elements was selected as the active antennas, i.e., 16 feeds in total. Employing the dual-polarized antennas helps to estimate channel parameters in polarization domain. The antenna pattern was obtained from Satimo SG128 antenna measurement system [22]. The measurement settings are summarized in Table 1.

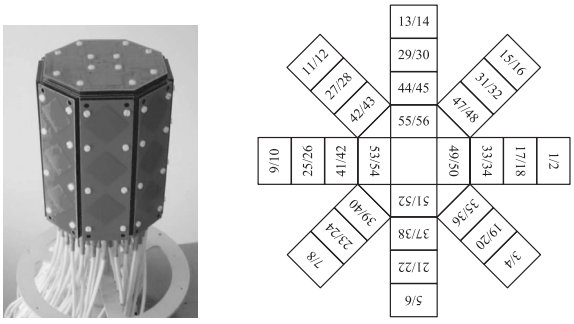

(a) Picture of ODA (b) Schematic plot of ODA

Fig. 1 Dual-polarized omnidirectional array used in measurements.

Table 1 Measurement parameters.

Items	Settings
Carrier Frequency (GHz)	2.35
Bandwidth (MHz)	50
Code length (chips)	255
Transmitting power (dBm)	26
Types of antennas	ODA
Number of active antennas at BS	16
Number of active antennas at RS	16
Number of active antennas at MS	16
Height of BS antenna (m)	22
Height of RS antenna (m)	7
Height of MS antenna (m)	1.8

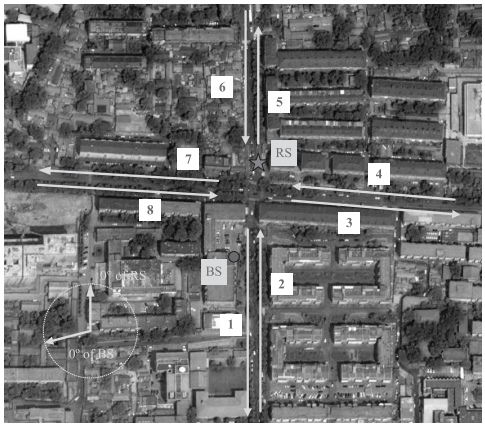

Fig. 2 Vertical view of measurement scenario. The circle mark indicates the position of the BS, while the star mark indicates the position of the RS. The straight links with arrow denote routes of the MS, and the arrow indicates the movement direction of the MS, which is opposite to the 0° direction of the antenna.

2.2 Environment

The measurement was carried out in a typical urban area of Beijing, China. The measurement scenario is illustrated in Fig. 2. The measurement area is characterized by buildings ranging from 4 to 5 floors. Antennas of the BS were placed on the roof top of a 5-floor building, which is about 22 m in height. To agree with the practical application scenario, the height of RS antennas was set to around 7 m above the street. In addition, LOS propagation exists between the BS

and the RS. The horizontal distance between the BS and the RS is 107 m. The MS antennas were mounted on a trolley. The height of the MS antennas was adjusted to about 1.8 m in order to imitate the height of human body. By moving the MS antennas, eight continuous routes were measured. In the RS-MS link, routes 1, 2, 5, 6 are in the LOS propagation environment, and routes 3, 4, 7, 8 are in the NLOS propagation environment. The positions of MS were recorded by Global Positioning System (GPS).

3. Data Post-Processing

Data post-processing consists of three procedures: (1) obtaining CIR from measured raw data, (2) estimating channel parameters using space-alternating generalized expectation (SAGE) algorithm, and (3) partitioning estimated parameters into local areas (LAs) according to position information of the MS.

3.1 Channel Impulse Response

Raw data collected by the receiver of channel sounder are the spread signals with the system impulse response of the sounding system. The system impulse response, which was obtained from the calibration of the sounder, was removed from raw data. Then, CIRs were calculated through the cyclic correlation with the known PRBS.

Since the noise level P_{noise} varies with time, the noise level estimation was done for each measurement cycle. To ensure that the signal is much stronger than the noise so that the additive noise does not affect the inherent characteristic of the channel, a threshold P_{th} was then determined by both the estimated noise level P_{noise} and the peak power of CIRs P_{peak},

$$P_{\text{th}} = \max\left\{P_{\text{noise}} + D_{\text{m}}, P_{\text{peak}} - D_{\text{r}}\right\}, \tag{1}$$

where D_{m} is the noise margin from noise floor P_{noise}, and D_{r} denotes the dynamic range from the peak power P_{peak}. Paths with power below the threshold P_{th} were ignored. The dynamic range D_{r} was set to 25 dB and the margin D_{m} was set to 6 dB, empirically.

3.2 Signal Model

Consider an $M \times N$ MIMO channel, the component contributed by the ℓth multipath component (MPC) to the signal at the output of receive array can be modeled as

$$\begin{aligned}\mathbf{s}(t;\boldsymbol{\theta}_\ell) &\doteq [s_1(t;\boldsymbol{\theta}_\ell), \ldots, s_M(t;\boldsymbol{\theta}_\ell)]^{\text{T}} \\ &= \exp\{j2\pi\nu_\ell t\}\mathbf{C}_2(\boldsymbol{\Omega}_{2,\ell})\mathbf{A}_\ell\mathbf{C}_1(\boldsymbol{\Omega}_{1,\ell})^{\text{T}}\mathbf{u}(t-\tau_\ell).\end{aligned} \tag{2}$$

The MPCs can be described by a parameter set $\boldsymbol{\theta} \doteq \{(\boldsymbol{\Omega}_{1,\ell}, \boldsymbol{\Omega}_{2,\ell}, \tau_\ell, \nu_\ell, \mathbf{A}_\ell)\colon \ell = 1, 2, \ldots, L\}$. $\boldsymbol{\Omega}_{1,\ell}, \boldsymbol{\Omega}_{2,\ell}, \tau_\ell, \nu_\ell, \mathbf{A}_\ell$ denote, respectively, the angle of departure (AOD), the angle of arrival (AOA), the propagation delay, the Doppler shift and the polarization matrix. The reference angle of angular estimation results is the boresight of the antennas. The polarization matrix of the ℓth MPC, $\mathbf{A}_\ell$, reads

$$\mathbf{A}_\ell \doteq \begin{bmatrix} \alpha_{\ell,V,V} & \alpha_{\ell,V,H} \\ \alpha_{\ell,H,V} & \alpha_{\ell,H,H} \end{bmatrix}. \tag{3}$$

The entry $\alpha_{\ell,p,q}$, $p, q \in \{V, H\}$ is the complex gain of q-to-p polarization of the ℓth MPC. $\mathbf{C}_k(\boldsymbol{\Omega}) = [\boldsymbol{c}_{k,1}(\boldsymbol{\Omega}), \boldsymbol{c}_{k,2}(\boldsymbol{\Omega})]$, $k \in \{1, 2\}$, is the complex response of the kth antenna array. $\boldsymbol{c}_{k,1}(\boldsymbol{\Omega})$ is in the vertical polarization, while $\boldsymbol{c}_{k,2}(\boldsymbol{\Omega})$ is in the horizontal polarization.

3.3 Channel Parameter Estimation

SAGE algorithm [23] is used to extract the channel parameters. SAGE is based on the maximum likelihood method and allows joint estimation of the parameter set $\boldsymbol{\theta} \doteq \{(\boldsymbol{\Omega}_{1,\ell}, \boldsymbol{\Omega}_{2,\ell}, \tau_\ell, \nu_\ell, \mathbf{A}_\ell)\colon \ell = 1, 2, \ldots, L\}$ from the CIRs. In order to extract all dominant paths to exactly characterize the propagation environment, 30 MPCs with strongest power are estimated in each measurement cycle, namely, $L = 30$.

3.4 Local Area Partitioning

The longitude-latitude coordinates recorded by GPS are converted into 2D-Cartesian coordinates with the Tx position of the link as the origin. Let $\boldsymbol{r} = (x, y)$ be the vector indicating Rx location of the link at any instance. Correspondingly, $\|\boldsymbol{r}\|$ denotes the distance between the Tx and the Rx. Define the LA of position $\boldsymbol{r}$ as the circular range centered at position $\boldsymbol{r}$ with a constant radius R, and let $\mathcal{A}(\boldsymbol{r}; R) = \{s_1, s_2, \ldots, s_K\}$ be the set of measurement positions within the LA of position $\boldsymbol{r}$, where K is the cardinality of $\mathcal{A}(\boldsymbol{r}; R)$. For every $s_i \in \mathcal{A}(\boldsymbol{r}; R)$, $i = 1, 2, \ldots, N$, there exists a parameter set $\boldsymbol{\theta}_i = \{(\boldsymbol{\Omega}_{1,\ell}, \boldsymbol{\Omega}_{2,\ell}, \tau_\ell, \nu_\ell, \mathbf{A}_\ell)\colon \ell = 1, 2, \ldots, L\}$, $L = 30$. We collect these $\boldsymbol{\theta}_i$ to construct a new parameter set $\boldsymbol{\Theta}(\boldsymbol{r}, R)$, which corresponds to the LA with centered at $\boldsymbol{r}$. We use the parameters in $\boldsymbol{\Theta}(\boldsymbol{r}, R)$ to investigate the statistics of channels at position $\boldsymbol{r}$, i.e., $\mathbf{H}(\boldsymbol{r})$. In our analysis, the R is set to 20λ, where λ is the wavelength.

4. Measurement Results and Analysis

In this section, the measurement and analysis results are presented. The channel statistics in polarization and spatial domain are firstly obtained, and the corresponding distributions for XPD and PAS are proposed. Then, a closed-form approximation of the channel correlation, which takes into consideration the impact of XPD and PAS, is derived to investigate the channel correlation. Based on typical channel parameters measured from the LOS and NLOS scenarios, the channel correlation values of uni- and dual-polarized antenna arrays are assessed.

4.1 Polarization Statistics

4.1.1 The Distribution of the XPD

XPD has an important influence on the diversity gain [17].

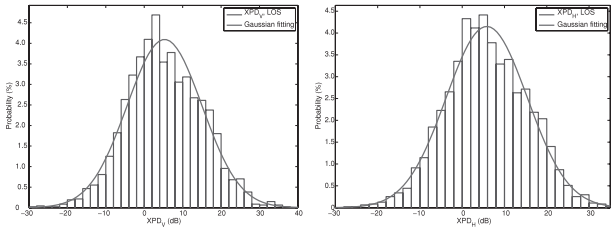

(a) XPD_V for LOS (b) XPD_H for LOS

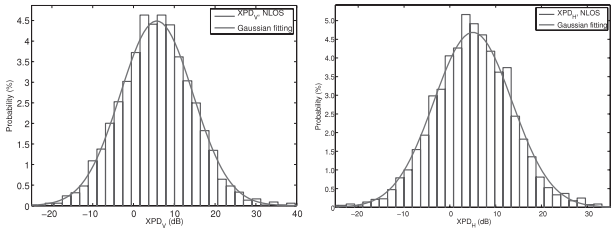

(c) XPD_V for NLOS (d) XPD_H for NLOS

Fig. 3 The distribution of XPD and corresponding Gaussian fitting for $\boldsymbol{\Theta}(\boldsymbol{r}, R)$ with $\|\boldsymbol{r}\| = 25$ m in LOS andNLOS scenarios.

Table 2 Gaussian fitting parameters in RS-MS link for $\boldsymbol{\Theta}(\boldsymbol{r}, R)$ with $\|\boldsymbol{r}\| = 25$ m.

	LOS		NLOS	
	XPD_V	XPD_H	XPD_V	XPD_H
μ	5.3	5.2	5.7	5.0
σ	9.7	9.6	8.8	8.5

XPD is defined as the co-polarized received signal power to the cross-polarized received power, which is given by

$$\mathrm{XPD_V} = 10 \cdot \log_{10}\left(\left|\frac{\alpha_{V,V}}{\alpha_{H,V}}\right|^2\right)(\mathrm{dB}), \tag{4}$$

$$\mathrm{XPD_H} = 10 \cdot \log_{10}\left(\left|\frac{\alpha_{H,H}}{\alpha_{V,H}}\right|^2\right)(\mathrm{dB}). \tag{5}$$

The XPD value of every path in one LA is calculated according to (4) and (5). About 900 values of XPD can be gotten in one LA. Then, the set of all XPD values is used to estimate the distribution of the XPD. Thus, the obtained distribution is independent of the AOA and AOD.

The distribution of the XPD can be modeled as XPD $\sim \mathcal{N}(\mu, \sigma^2)$ [24]. The XPD_V and XPD_H for both LOS and NLOS scenarios in RS-MS link are shown in Fig. 3. It can be found that both XPD_V and XPD_H fit Gaussian distribution very well. The mean value μ and standard deviation σ of the least square fitting are given in Table 2. It can be observed that, when the distance from the RS to the MS is 25 m, the distribution of XPD_V and XPD_H for LOS case manifests similar mean values and standard deviations. For NLOS case, the mean value of XPD_V is larger than that of XPD_H. The results indicate that the vertical polarization preserves better than the horizontal polarization during the propagation when the scatters are rich. Furthermore, we find that the standard deviation of LOS scenario is larger than that of NLOS scenario.

Table 3 The parameters a and n for XPD_V and XPD_H.

	LOS		NLOS	
	XPD_V	XPD_H	XPD_V	XPD_H
a	5.3	5.2	5.7	5.0
n	0.22	−0.14	0.34	−0.52

4.1.2 Dependence of XPD on Distance

For outdoor environments, the dependence of XPD on distance in conventional BS-MS link was reported by [25]. For indoor environments, the relation between XPD and distance was discussed in [24], [26]. In [26], the exponential law was used. On the contrast, the power law was adopted by [24]. The applicability of different models was attributed to the propagation characteristics [26]. When there are rich local scatters, the power law applies, and vice versa. In the RS-MS link, both the RS and the MS antennas are surrounded by local scatters due to lower height of RS antennas. Based on the results of least square fitting, we find that the relation between XPD and distance can be best described by the power law, especially for NLOS scenarios. The XPD as a function of distance can be modeled as

$$\mathrm{XPD}(d)\big|_{\mathrm{dB}} = a + n \cdot 10\log_{10}\left(\frac{d}{d_0}\right), \tag{6}$$

where n is the exponent indicating the rate at which the XPD varies with the distance, $25 \le d \le 300$ is the separation distance in meters, d_0 is the reference distance and $a = \mathrm{XPD}\big|_{d_0=25m}$. The constants a and n for modeling the dependence of XPD in different polarization on the distance are given in Table 3. It can be observed that the XPD_V and XPD_H manifest different changing trends over distance. The XPD_V increases as the distance increases, while the XPD_H decreases. The reason is that the complex gains of q-to-p, $p, q \in \{V, H\}$ polarization fall off at different rates. From the changing trends of XPD_V and XPD_H, we conclude that the complex gain of V-to-H polarization falls off faster than that of V-to-V polarization. Similarly, the complex gain of H-to-H polarization decays faster than that of H-to-V polarization. The difference between XPD_V and XPD_H is more obvious for NLOS case than for LOS case. The results reveal that the vertical polarization preserves better than the horizontal polarization during the propagation, especially in the RS-MS link where the RS antennas height is relatively lower. Based on the Table 3, an empirical formula for predicting the difference between XPD_V and XPD_H can be given as follows

$$\begin{aligned}\mathrm{XPD}_{dif}(d) &= \mathrm{XPD_V}(d) - \mathrm{XPD_H}(d) \\ &= \begin{cases} 3.6 \cdot \log_{10}(d) - 4.1, & \text{for LOS,} \\ 8.6 \cdot \log_{10}(d) - 11.3, & \text{for NLOS,} \end{cases}\end{aligned} \tag{7}$$

4.1.3 Comparison of XPDs in BS-RS and RS-MS Links

The mean value and standard deviation of BS-RS link were

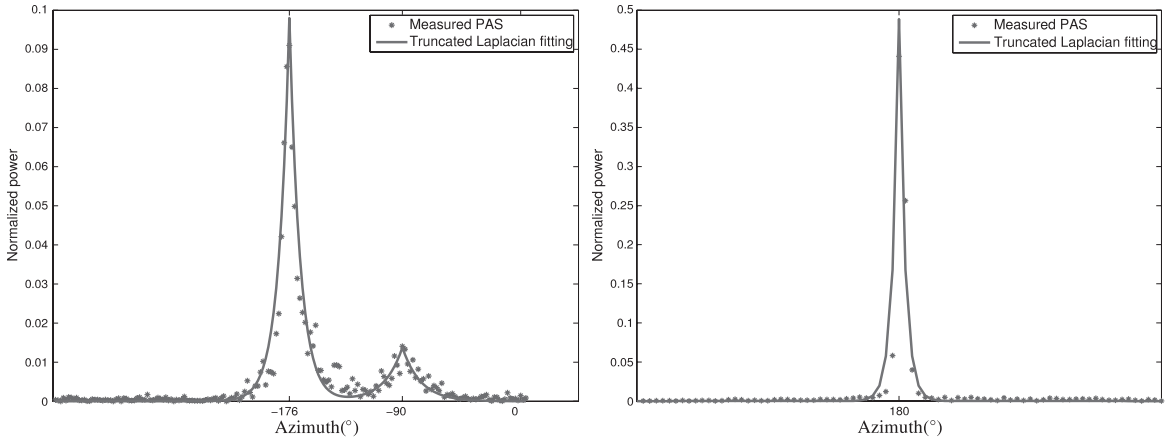

(a) PAS of Rx (b) PAS of Tx

Fig. 4 Measured PAS and corresponding multi-cluster truncated Laplacian fitting in LOS scenario.

also obtained using (4) and (5). In the BS-RS link, the MPCs that arrive at the RS undergo less scatters due to the larger height of the BS antennas. The μ and σ of XPD_V for BS-RS link are 9.1 dB and 8.0 dB, while the μ and σ of XPD_H for the BS-RS link are 6.0 dB and 9.0 dB. As mentioned in Sect. 2.2, the distance from the BS to the RS is 107 m. The mean values of XPD_V and XPD_H in the RS-MS link with the same separation distance, which are calculated based on Table 3, are 9.6 dB and 2.6 dB, respectively. While the XPD_V values in BS-RS and RS-MS links are almost the same, the XPD_H values in RS-MS link are much smaller.

4.2 Spatial Characteristics

4.2.1 The Distribution of PAS

PAS, from which the information about the scattering objects can be derived, is an important statistical property of the wireless channel, since it directly influences the Doppler power spectrum and the spatial correlation of the wireless MIMO channel. The truncated Laplacian distribution has been introduced in [27] as the best fit to measured PAS in urban and rural areas for the conventional BS-MS link. The truncated Laplacian distribution can be expressed as

$$p_\phi(\phi)=\begin{cases}\dfrac{\eta_\phi}{\sqrt{2}\sigma_\phi}\cdot\exp\left(-\dfrac{\sqrt{2}|\phi-\phi_0|}{\sigma_\phi}\right), & \text{for } \phi\in[-\pi,\pi),\\ 0, & \text{otherwise,}\end{cases} \tag{8}$$

where ϕ is the azimuth, $\phi_0 \in [\pi, \pi)$ is the mean angle, $\eta_\phi = 1/(1-e^{-\sqrt{2}\pi/\sigma_\phi})$ is the normalized factor, and σ_ϕ is the root-mean-square (RMS) angular spread (AS). The AS in the kth cluster can be calculated as [28]

$$\sigma_k = \min_{\Delta}\sigma_k(\Delta) = \sqrt{\sum_{n=1}^{N_k}(\theta_{n,u}(\Delta))^2\cdot P_n \Big/ \sum_{n=1}^{N_k} P_n}, \tag{9}$$

where N_k is the number of MPCs in the kth cluster, P_n is the power of the nth path and $\Delta \in [-\pi, \pi)$ is the compensation angle. $\theta_{n,\mu}$ is defined as

$$\theta_{n,\mu}(\Delta)=\begin{cases}2\pi+(\theta_n(\Delta)-\mu_\theta(\Delta)) & (\theta_n(\Delta)-\mu_\theta(\Delta)) < -\pi\\ (\theta_n(\Delta)-\mu_\theta(\Delta)) & |(\theta_n(\Delta)-\mu_\theta(\Delta))| < +\pi\\ 2\pi-(\theta_n(\Delta)-\mu_\theta(\Delta)) & (\theta_n(\Delta)-\mu_\theta(\Delta)) > +\pi\end{cases}, \tag{10}$$

where $\mu_\theta(\Delta)$ is defined as $\mu_\theta(\Delta) = \sum_{n=1}^{N_k}\theta_n(\Delta)\cdot P_n / \sum_{n=1}^{N_k} P_n$ and $\theta_n(\Delta) = \theta_n + \Delta$.

The measured PASs in RS-MS link for $\Theta(\boldsymbol{r}, R)$ with $\|\boldsymbol{r}\| = 50$ m are illustrated in Figs. 4 and 5. It can be found that for LOS case, the PAS at the RS side fits the Laplacian distribution. The MPCs departing the RS gather in one cluster with small AS. However, at the MS side, besides the cluster introduced by the LOS propagation, another cluster appears with mean angle of 90°. For the NLOS case, the PASs in both RS and MS sides consist of two dominating clusters and the clusters overlap. Thus, we propose a multi-cluster Laplacian distribution for modeling the measured PAS. The PAS of multi-cluster Laplacian distribution was observed in our previous measurements in the indoor hotspot scenarios [29]. We attribute the observed phenomenon in our measurement to the lower height of RS antennas. In the RS-MS link, both the RS and MS antennas are surrounded by local scatters, which yields a link with rich scatters. The multi-cluster Laplacian distribution can be expressed as

$$\begin{aligned}p_\phi &= \sum_{n=1}^{N_C} p_\phi^n\\ &= \begin{cases}\displaystyle\sum_{n=1}^{N_C}\frac{Q^n\eta_\phi^n}{\sqrt{2}\sigma_\phi^n}\exp\left(-\frac{\sqrt{2}|\phi-\phi_0^n|}{\sigma_\phi^n}\right), & \text{for } \phi\in[-\pi,\pi),\\ 0, & \text{otherwise,}\end{cases}\end{aligned} \tag{11}$$

where N_C is the number of clusters, $\phi_0^n \in [-\pi, \pi)$ is the mean angle of the nth cluster, σ_ϕ^n is the AS in the nth cluster, Q^n is the ratio of the nth cluster power to the total power, and $\sum_{n=1}^{N_c} Q_n\eta_\phi^n = 1$. Parameters for describing PASs in Figs. 4 and 5 are shown in Table 4. The parameters of PASs in the

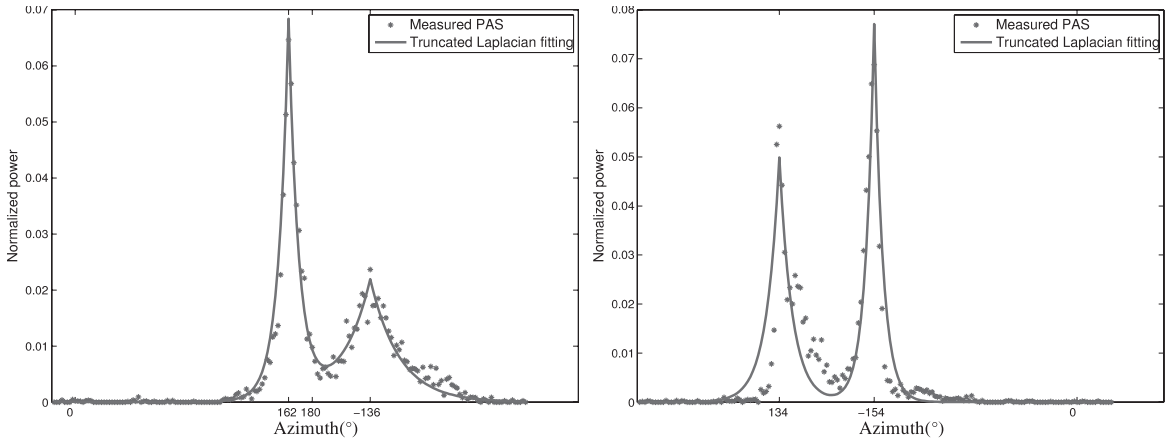

(a) PAS of Rx for NLOS scenario (b) PAS of Tx

Fig. 5 Measured PAS and corresponding multi-cluster truncated Laplacian fitting in NLOS scenario.

Table 4 Parameters for describing the distribution of PAS with $\|\boldsymbol{r}\|$ = 50 m.

	cluster index	Q^n	$\phi_0^n(^\circ)$	$\sigma_\phi^n(^\circ)$
BS-RS,LOS,Tx	cluster 1	1	−113	3.5
BS-RS,LOS,Rx	cluster 1	1	151	3.2
RS-MS,LOS,Tx	cluster 1	1	180	2.6
RS-MS,LOS,Rx	cluster 1	0.80	−176	11.6
	cluster 2	0.20	−90	19.6
RS-MS,NLOS,Tx	cluster 1	0.52	−154	9.4
	cluster 2	0.48	134	13.7
RS-MS,NLOS,Rx	cluster 1	0.52	162	10.8
	cluster 2	0.48	−136	31.2

Table 5 Parameters for describing the distribution of PAS with $\|\boldsymbol{r}\|$ = 200 m.

	cluster index	Q^n	$\phi_0^n(^\circ)$	$\sigma_\phi^n(^\circ)$
RS-MS,LOS,Tx	cluster 1	1	−178	1.0
RS-MS,LOS,Rx	cluster 1	1	−172	5.0
RS-MS,NLOS,Tx	cluster 1	0.50	142	11.4
	cluster 2	0.49	−160	9.8
RS-MS,NLOS,Rx	cluster 1	0.57	174	7.5
	cluster 2	0.31	162	8.5
	cluster 3	0.11	−132	6.8

BS-RS link are also included. The small ASs at both the BS and RS side imply that the LOS propagation is dominant and the contribution from all the scatters is small.

To investigate the trend of PAS against the distance, the parameters for describing the PAS in $\Theta(\boldsymbol{r}, R)$ with $\|\boldsymbol{r}\|$ = 200 m are given in Table 5 gives. It can be found that in the case of the LOS scenario, the ASs in the cluster at both the RS and the MS side decrease as the distance increases. The number of the clusters at the MS side reduces to 1. This is mainly because MPCs attenuate more after traveling for longer distance and undergoing more interaction with the scatterers. Only MPCs with stronger power survive, and MPCs become more concentrated. In the case of the NLOS scenario, the ASs in the cluster at the RS side show little change when the distance increases to 200 m. However, the number of clusters at the MS side increases to 3, and the ASs in the cluster increase.

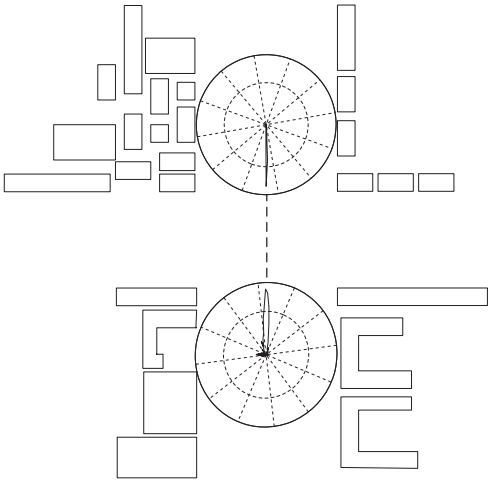

Fig. 6 Illustration of measured PAS for $\Theta(\boldsymbol{r}, R)$ with $\|\boldsymbol{r}\|$ = 50 m in LOS scenarios for the analysis of propagation mechanism.

4.2.2 Propagation Mechanisms

We import the measured PAS into the site-map to investigate the relationship between the propagation environment and the PAS. Examples of measured PAS results are shown in Fig. 6 for LOS propagation and in Fig. 7 for NLOS propagation. With the data in Tables 4 and 5, the following observations are made:

1. *LOS scenario*: As shown in Fig. 6, when the LOS exists, the strongest cluster always comes from the direction of LOS. The first-order reflected MPCs from buildings along the street also contribute to the PAS (cluster 2 of Rx PAS in RS-MS link for the case of LOS, in Table 4). The order of reflection refers to the number of reflections that MPC goes through before it reaches the receiver. At the MS side, the cluster introduced by the LOS (cluster 1 of Rx PAS in RS-MS link for the case of LOS, in Table 4) has a significantly

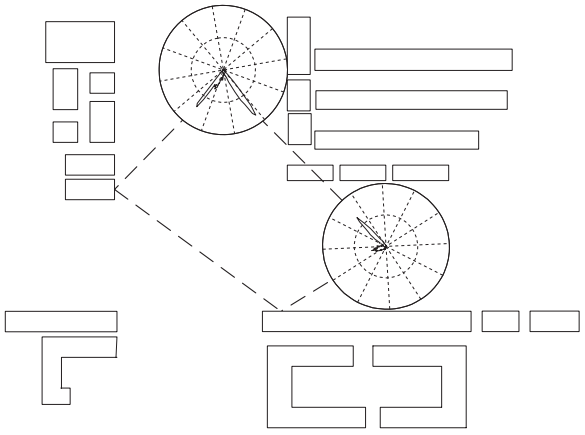

Fig. 7 Illustration of measured PAS for $\Theta(\boldsymbol{r}, R)$ with $\|\boldsymbol{r}\| = 50$ m in NLOS scenarios for the analysis of propagation mechanism.

higher power than the cluster caused by the first-order reflection. 80% of the total power are in cluster 1. Analyzing the cluster parameters in Table 5 helps to gain insight into the propagation mechanism as the distance increases. The reduction of the cluster number at the MS side indicates that the LOS propagation becomes more dominant. The contribution from all the scatters can be neglected.

2. *NLOS scenario*: It can be observed from Fig. 7 that the PAS seems to be more diffuse compared to the LOS propagation. The diffraction at the edges of roofs and the second-order reflection contribute to the majority of the PAS. The cluster introduced by diffraction (cluster 1 in RS-MS link for the case of NLOS, in Table 4) has larger power than the cluster caused by the second-order reflection (cluster 2 in RS-MS link for the case of NLOS, in Table 4). The two clusters show similar power, i.e., 52% in cluster 1 and 48% percent in cluster 2. As the distance increases, the cluster number at the MS side increases to 3, which implies a complicated propagation mechanism. After importing the PAS into the site-map, it can be inferred from the mean angles of the clusters (see Table 5) that the clusters are also generated by the diffraction and second-order reflection.

Therefore we can conclude that in the RS-MS link, the LOS propagation is the dominating propagation mechanisms in LOS scenarios. When the MS is near the RS, the first-order propagation is also an important propagation mechanism. Meanwhile, the diffraction from the roofs and second-order reflection are main propagation mechanisms in NLOS scenarios.

4.3 Channel Correlation

In this section, we investigate the channel correlation of the BS-RS and RS-MS links. When polarized antennas are adopted, the channel correlation is contributed by both spatial and polarization correlation. In order to make our results applicable to a more flexible geometry of the antenna, we use the field pattern model for slanted dipole antennas in [24]. The antenna responses in vertical and horizontal polarization, namely $\boldsymbol{c}_1(\phi)$ and $\boldsymbol{c}_2(\phi)$, are given by

$$\begin{cases} \boldsymbol{c}_1(\phi) &= \cos\theta, \\ \boldsymbol{c}_2(\phi) &= \sin\theta\cos\phi, \end{cases} \tag{12}$$

where ϕ is the azimuth and θ is the slanted angle with reference to vertical plane. For the case when only single cluster exists in PAS and slanted antennas with certain spacing are employed, the intermediate results of the channel correlation were given in [30]. The covariance between the (u, s) and (u', s') antenna pairs can be obtained as

$$r_{us}^{u's'} \approx P_n \cdot \mathbf{c}_{us}^{u's'} \cdot \mathbf{K} \cdot \mathbf{y}(\phi, \varphi), \tag{13}$$

where

$$\mathbf{K} = \mathrm{diag}(1, \kappa_1, \kappa_2, 1) \tag{14}$$

$$\mathbf{c}_{us}^{u's'} = \begin{pmatrix} c_{11} \\ c_{12} \\ c_{21} \\ c_{22} \end{pmatrix}^{\mathrm{T}} = \begin{pmatrix} \cos\theta_s \cos\vartheta_u \cos\theta_{s'} \cos\vartheta_{u'} \\ \cos\theta_s \sin\vartheta_u \cos\theta_{s'} \sin\vartheta_{u'} \\ \sin\theta_s \cos\vartheta_u \sin\theta_{s'} \cos\vartheta_{u'} \\ \sin\theta_s \sin\vartheta_u \sin\theta_{s'} \sin\vartheta_{u'} \end{pmatrix}^{\mathrm{T}} \tag{15}$$

$$\mathbf{y}(\phi, \varphi) = \left(y_\phi^{(1)} y_\varphi^{(1)} \quad y_\phi^{(1)} y_\varphi^{(2)} \quad y_\phi^{(2)} y_\varphi^{(1)} \quad y_\phi^{(2)} y_\varphi^{(2)} \right)^{\mathrm{T}}, \tag{16}$$

$$y_\phi^{(1)} = \int_{-\pi}^{\pi} p_\phi(\phi) \exp[jk\Delta d_{\mathrm{Tx}} (\phi_0 - \phi)] d\phi, \tag{17}$$

$$y_\varphi^{(1)} = \int_{-\pi}^{\pi} p_\varphi(\varphi) \exp[jk\Delta d_{\mathrm{Rx}} (\varphi_0 - \varphi)] d\varphi, \tag{18}$$

$$y_\phi^{(2)} = \int_{-\pi}^{\pi} p_\phi(\phi) \cos^2(\phi_0 - \phi) \exp[jk\Delta d_{\mathrm{Tx}} (\phi_0 - \phi)] d\phi, \tag{19}$$

$$y_\varphi^{(2)} = \int_{-\pi}^{\pi} p_\varphi(\varphi) \cos^2(\varphi_0 - \varphi) \exp[jk\Delta d_{\mathrm{Rx}} (\varphi_0 - \varphi)] d\varphi, \tag{20}$$

where k is the wave number $2\pi/\lambda$, $\kappa_i, i \in \{1, 2\}$ are the inverse of the XPD in vertical and horizontal polarization, $\theta_j, j \in \{u, u'\}, \vartheta_k, k \in \{s, s'\}$ are the slanted angle of Tx and Rx antennas, $\Delta d_l, l \in \{\mathrm{Tx}, \mathrm{Rx}\}$ are the wave-path difference between antennas, and $p_m(m), m \in \{\phi, \varphi\}$ are the PAS of Tx and Rx. Note that here the reference angle of ϕ and φ are the mean angle ϕ_0 and φ_0, respectively. The closed-form solution of (13) when the antenna spacing is nonzero was not given in [30]. We extend the expression to a general case when multiple clusters exist and give a closed-form expression. For the PAS of multi-cluster Laplacian distribution, the $y_\phi^{(1)}$, $y_\phi^{(2)}$, $y_\varphi^{(1)}$ and $y_\varphi^{(2)}$ can be calculated as (22), (23), (24) and (25). The detailed derivation is given in the Appendix. Then, the channel correlation coefficient $\rho_{us}^{u's'}$ can be calculated as

$$\rho_{us}^{u's'} = \frac{r_{us}^{u's'}}{\sigma_{us}\sigma_{u's'}}, \tag{21}$$

where $\sigma_{us}^2 = r_{us}^{us}|_{\Delta d_{\mathrm{Tx}}=\Delta d_{\mathrm{Rx}}=0}$ and $\sigma_{u's'}^2 = r_{u's'}^{u's'}|_{\Delta d_{\mathrm{Tx}}=\Delta d_{\mathrm{Rx}}=0}$. We

$$y_{\phi}^{(1)} = \sum_{n=1}^{N_C} Q_n \eta_{\phi}^{n} \exp\left[jkd\,(u-u')\sin(\phi_0^n)\right] \cdot \frac{2}{2+\left[\sigma_{\phi}^{n} kd\,(u-u')\cos(\phi_0^n)\right]^2} \tag{22}$$

$$y_{\varphi}^{(1)} = \sum_{n=1}^{N_C} Q_n \eta_{\varphi}^{n} \exp\left[jkd\,(s-s')\sin(\varphi_0^n)\right] \cdot \frac{2}{2+\left[\sigma_{\varphi}^{n} kd\,(s-s')\cos(\varphi_0^n)\right]^2} \tag{23}$$

$$y_{\phi}^{(2)} = \frac{1}{2}\sum_{n=1}^{N_C} Q_n \eta_{\phi}^{n} \exp\left[jkd\,(u-u')\sin(\phi_0^n)\right] \left[\begin{array}{c}\left(\frac{2}{2+\left[\sigma_{\phi}^{n} kd(u-u')\cos(\phi_0^n)\right]^2}\right) + \exp\left(-j2\phi_0^n\right)\left(\frac{1}{2+\left[2\sigma_{\phi}^{n}+kd(u-u')\cos(\phi_0^n)\sigma_{\phi}^{n}\right]^2}\right) \\ + \exp\left(j2\phi_0^n\right)\left(\frac{1}{2+\left[2\sigma_{\phi}^{n}-kd(u-u')\cos(\phi_0^n)\sigma_{\phi}^{n}\right]^2}\right)\end{array}\right] \tag{24}$$

$$y_{\varphi}^{(2)} = \frac{1}{2}\sum_{n=1}^{N_C} Q_n \eta_{\varphi}^{n} \exp\left[jkd\,(s-s')\sin(\varphi_0^n)\right] \left[\begin{array}{c}\left(\frac{2}{2+\left[\sigma_{\varphi}^{n} kd(s-s')\cos(\varphi_0^n)\right]^2}\right) + \exp\left(-j2\varphi_0^n\right)\left(\frac{1}{2+\left[2\sigma_{\varphi}^{n}+kd(s-s')\cos(\varphi_0^n)\sigma_{\varphi}^{n}\right]^2}\right) \\ + \exp\left(j2\varphi_0^n\right)\left(\frac{1}{2+\left[2\sigma_{\varphi}^{n}-kd(s-s')\cos(\varphi_0^n)\sigma_{\varphi}^{n}\right]^2}\right)\end{array}\right] \tag{25}$$

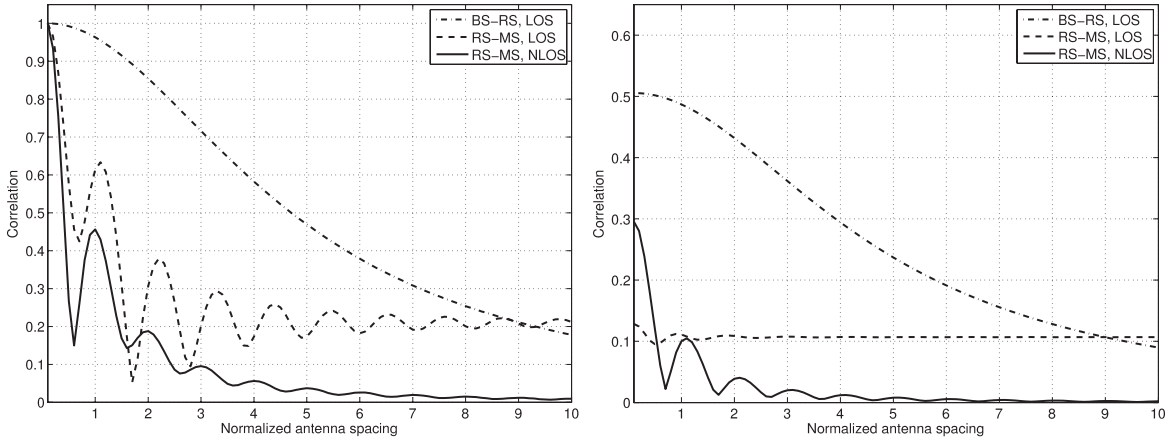

(a) Case I : spatial correlation (b) Case II : the combination of spatial and polarization correlation

Fig. 8 The channel correlation for both LOS and NLOS scenarios at the Rx side.

use the parameters in Table 4 and XPDs of corresponding measurement location to evaluate the channel correlation. The following two antenna configurations are studied. In case I, the vertical polarized antennas were used at both Tx and Rx sides, i.e., $\theta_u = \theta_{u'} = \vartheta_s = \vartheta_{s'} = 0^\circ$, where the channel correlation is only contributed by spatial correlation. In case II, $\theta_u = \theta_{u'} = -45^\circ$, $\vartheta_s = -45^\circ$, and $\vartheta_{s'} = +45^\circ$, then the channel correlation includes both spatial and polarization correlation. The diversity gain could be obtained if the correlation is less than $\rho \leq 0.5$ [31]. We define the distance beyond which the correlation is lower than 0.5 as *correlation space*.

Assuming $\Delta d_{\mathrm{Tx}} = 0$, namely, there is no spacing between the uth and u'th Tx antennas, the absolute values of correlation coefficient $|\rho_{us}^{u's'}|$ as a function of Δd_{Rx} for BS-RS and RS-MS links are given in Figs. 8(a) and 8(b). It can be observed from Fig. 8(a) that for case I, due to the small AS, the correlation in BS-RS link decreases slowly as the Δd_{Rx} increases. The correlation space is 4.6λ, which implies that in the system implementation, the dimension of the antennas needs to be large in order to reduce the correlation between channels. For the LOS case in the RS-MS link, the correlation curve is lower than 0.5 once the Δd_{Rx} is larger than 1.5λ. As the Δd_{Rx} increases, the curve oscillates around the value 0.2. For the NLOS case in the RS-MS link, the correlation curve falls down rapidly owing to the larger AS. The corresponding Δd_{Rx} is about 0.3λ when the correlation is 0.5. We can see that for NLOS case in the RS-MS link, the correlation can be reduced to be low enough under the constraint of the antenna array dimension. However, this is not the case for BS-RS and RS-MS link under LOS propagation condition. For LOS case, the size of antennas arrays needs to be fairly big to meet the requirement of low channel correlation. From Fig. 8(b), it can be found that the correlation shows an significant reduction in case II. The correlation space of BS-MS link for LOS case is 1.8λ. The channel correlation values in RS-MS link are below 0.5 for all Δd_{Rx}.

The absolute values of correlation coefficient $|\rho_{us}^{u's'}|$ as a function of Δd_{Tx} for BS-RS and RS-MS links are given

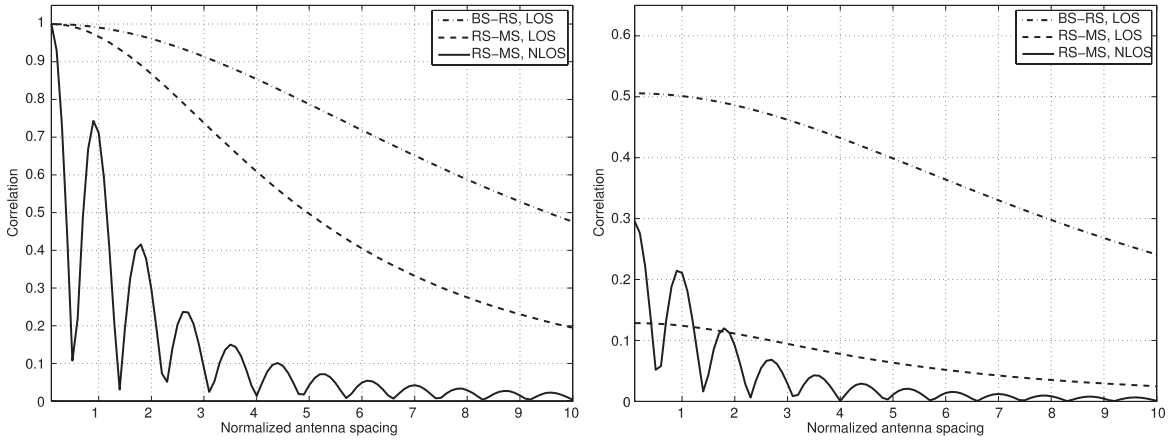

(a) Case I : spatial correlation (b) Case II : the combination of spatial and polarization correlation

Fig. 9 The channel correlation for both LOS and NLOS scenarios at the Tx side.

in Figs. 9(a) and 9(b), assuming there is no spacing between the sth and s'th Rx antennas. From the comparison of Figs. 4 and 5, we can see the AS at the Tx side is smaller than that at the Rx side. As expected, the channel correlation is higher than that at the Rx side with the same separation (see Figs. 8(a) and 9(a)). However, comparing Fig. 8(b) with 9(b), we find that when utilizing the dual-polarized antennas, the channel correlation at the Tx side is equivalent to or even lower than that at the Rx side, which reveals that the reduction of channel correlation is more significant. Therefore, we conclude that adopting antennas of different polarization performs better when the AS is small than when the AS is large.

The results above indicate that for the dimension-limited RS and MS, employing cross-polarized antennas is an effective way to fulfill the requirement of low correlation, especially when the AS is small. The constraint on the dimension of BS arrays is not as strict as that on the MS array, thus, flexible antenna configurations can be utilized at the BS according to the actual situation.

5. Conclusion

In this paper, the propagation statistics of MIMO relay channels are investigated based on outdoor measurements in IMT-Advanced frequency band (2.35 GHz with 50 MHz bandwidth). The polarization and spatial statistics are gotten based on parameters of MPCs, which are estimated using SAGE. First of all, the measurement and analysis results reveal different characteristics of the RS-MS link. The XPDs in different polarization, namely, $\mathrm{XPD_V}$ and $\mathrm{XPD_H}$, manifest different dependence on the separation distance between the RS and the MS. The $\mathrm{XPD_V}$ increases as the distance increases and the opposite for $\mathrm{XPD_H}$. The PASs of the RS-MS link agree well with the multi-cluster Laplacian distribution, which indicates the number of scatters increases due to the lower height of RS antennas. Based on the PAS, the propagation mechanisms in LOS and NLOS scenarios are studied. It is found that the LOS propagation and the first-order reflection are the main propagation mechanisms in LOS scenarios. While in NLOS scenarios, the diffraction from the roofs and high-order reflection are dominating. We attribute the different characteristics of RS-MS link to the lower height of RS antennas. Both the RS and MS antennas are surrounded by local scatters, which constitutes a link with rich scatters.

Furthermore, a approximate closed-form expression of channel correlation is derived. The expression takes into consideration the impact of both XPDs and PAS. The channel correlation for two antenna configurations is investigated. In case I when vertical polarized antennas are utilized, the channel correlation is high for LOS scenarios. The correlation spaces of BS-RS and RS-MS links are 4.6λ and 1.5λ, respectively. In case II when antennas of different polarization are used, the channel correlation decreases significantly. The correlation space reduces to 1.8λ for LOS scenarios in BS-RS link. The correlation values are all below 0.5 in the RS-MS link for all antenna separations. From the comparison of the correlations at Tx and Rx sides, we also observe that adopting dual-polarized antennas is more effective when the AS is small than when the AS is large. We can conclude that utilizing antennas of different polarization provides a rich MIMO solution for dimension-limited RS and MS.

Acknowledgements

This work was funded in part by China Important National Science and Technology Specific Projects with Grant No.2009ZX03007-003-01, National 863 High Technology Research and Develop Program of China with Grant NO.2009AA011502, and National Nature Science Foundation of China with NO.60772113.

References

[1] A. Nosratinia, T. Hunter, and A. Hedayat, "Cooperative communication in wireless networks," IEEE Commun. Mag., vol.42, no.10, pp.74–80, 2004.

[2] R. Pabst, B. Walke, D. Schultz, et al., "Relay-based deployment concepts for wireless and mobile broadband radio," IEEE Commun. Mag., vol.42, no.9, pp.80–89, 2004.
[3] M. Herdin, "MIMO amplify-and-forward relaying in correlated MIMO channels," Proc. 15th International Conference on Information, Communications and Signal Processing, pp.796–800, 2005.
[4] J. Laneman, G. Wornell, and D. Tse, "An efficient protocol for realizing cooperative diversity in wireless networks," Proc. IEEE International Symposium on Information Theory (ISIT'01), p.294, June 2001.
[5] R. Nabar, H. Bolcskei, and F. Kneubuhler, "Fading relay channels: Performance limits and space-time signal design," IEEE J. Sel. Areas Commun., vol.22, no.6, pp.1099–1109, Aug. 2004.
[6] P. Almers, E. Bonek, A. Burr, N. Czink, et al., "Survey of channel and radio propagation models for wireless MIMO systems," EURASIP J. Wireless Communications and Networking, vol.2007, Article ID 19070, 2007.
[7] Y. Karasawa, "Statistical multipath propagation modeling for broadband wireless systems," IEICE Trans. Commun., vol.E90-B, no.3, pp.468–484, March 2007.
[8] A. Molisch, L. Greenstein, and M. Shafi, "Propagation issues for cognitive radio," Proc. IEEE, vol.97, no.5, pp.787–804, 2009.
[9] P. Kyritsi, P. Eggers, R. Gall, et al., "Measurement based investigation of cooperative relaying," Proc. IEEE 64th Vehicular Technology Conference (VTC'06-Fall), pp.1–5, 2006.
[10] P. Kyritsi, P. Popovski, P. Eggers, et al., "Cooperative transmission: A reality check using experimental data," Proc. IEEE 65th Vehicular Technology Conference (VTC'07-Spring), pp.2281–2285, 2007.
[11] L. Jiang, L. Thiele, and V. Jungnickel, "Modeling and measurement of MIMO relay channels," Proc. IEEE 67th Vehicular Technology Conference (VTC'08-Spring), pp.419–423, 2008.
[12] K. Haneda, V.M. Kolmonen, T. Riihonen, et al., "Evaluation of relay transmission in outdoor-to-indoor propagation channels," Proc. COST2100 2nd Workshop on MIMO and Cooperative Communications, 2008.
[13] C. Oestges, N. Czink, B. Bandemer, et al., "Capacity performance of outdoor-to-indoor relay schemes in measured radio channels," Proc. IEEE 20th International Symposium on Personal, Indoor and Mobile Radio Communications (PIMRC'09), pp.1113–1117, 2009.
[14] P. Zetterberg, C. Mavrokefalidis, A.S. Lalos, et al., "Experimental investigation of cooperative schemes on a real-time DSP-based testbed," EURASIP Journal on Wireless Communications and Networking, vol.2009, Article ID 368752, 2009.
[15] J. Wagner, B. Rankov, and A. Wittneben, "Large n analysis of amplify-and-forward MIMO relay channels with correlated rayleigh fading," IEEE Trans. Inf. Theory, vol.54, no.12, pp.5735–5746, 2008.
[16] A. Paulraj, R. Nabar, and D. Gore, Introduction to Space-Time Wireless Communications, Cambridge University Press, 2003.
[17] N.K. Das, M. Shinozawa, N. Miyadai, et al., "Experiments on a MIMO system having dual polarization diversity branches," IEICE Trans. Commun., vol.E89-B, no.9, pp.2522–2529, Sept. 2006.
[18] M. Fukushige and T. Imai, "Analysis of polarization diversity gain at base station in W-CDMA system," IEICE Trans. Commun., vol.E90-B, no.9, pp.2360–2368, Sept. 2007.
[19] S. Ichitsubo, K. Tsunekawa, and Y. Ebine, "Multipath propagation model of spatio-temporal dispersion observed at base station in urban areas," IEEE J. Sel. Areas Commun., vol.20, no.6, pp.1204–1210, 2002.
[20] Elektrobit, "Propsound multidimensional channel sounder." http://www.propsim.com
[21] T. Pedersen, C. Pedersen, X. Yin, et al., "Optimization of spatiotemporal apertures in channel sounding," IEEE Trans. Signal Process., vol.56, no.10, pp.4810–4824, 2008.
[22] SATIMO, "Datasheet of SG 128 antenna measurement system." http://www.satimo.com/content/products/sg-128
[23] B. Fleury, M. Tschudin, R. Heddergott, et al., "Channel parameter estimation in mobile radio environments using the SAGE algorithm," IEEE J. Sel. Areas Commun., vol.17, no.3, pp.434–450, 1999.
[24] M. Shafi, M. Zhang, A. Moustakas, et al., "Polarized MIMO channels in 3D: Models, measurements and mutual information," IEEE J. Sel. Areas Commun., vol.24, no.3, pp.514–527, 2006.
[25] P. Soma, D. Baum, V. Erceg, et al., "Analysis and modeling of Multiple-Input Multiple-Output (MIMO) radio channel based on outdoor measurements conducted at 2.5 GHz for fixed BWA applications," Proc. IEEE International Conference on Communications 2002 (ICC'02), ed. 2, pp.272–276, 2002.
[26] P. Kyritsi, D. Cox, R. Valenzuela, et al., "Effect of antenna polarization on the capacity of a multiple element system in an indoor environment," IEEE J. Sel. Areas Commun., vol.20, no.6, pp.1227–1239, 2002.
[27] K. Pedersen, P. Mogensen, and B. Fleury, "Spatial channel characteristics in outdoor environments and their impact on BS antenna system performance," Proc. IEEE 48th Vehicular Technology Conference (VTC'98), vol.2, pp.719–723, 1998.
[28] 3GPP TR 25.996, "Spatial channel model for multiple input multiple output (MIMO) simulations (rel.6)," Tech. Rep., 2003.
[29] X. Nie, J. Zhang, Y. Zhang, et al., "An experimental investigation of wideband MIMO channel based on indoor hotspot NLOS measurements at 2.35 GHz," Proc. IEEE Global Telecommunications Conference 2008 (GLOBECOM'08), pp.1–5, 2008.
[30] Y. Zhang, J. Zhang, G. Liu, et al., "Impact of randomized cross-polarization discrimination on channel correlation property of the 3GPP spatial channel model," IEICE Trans. Commun., vol.E92.B, no.4, pp.1300–1307, April 2009.
[31] R. Vaughan and J. Andersen, "Antenna diversity in mobile communications," IEEE Trans. Veh. Technol., vol.36, no.4, pp.149–172, 1987.
[32] I. Gradshteyn and I. Ryzhik, Table of Integrals, Series, and Products, Academic Press, 2007.

Appendix: Derivation of (22), (23), (24) and (25)

This appendix is devoted to the derivation of (22), (23), (24) and (25). In the nth cluster, we choose the mean angle ϕ_0^n as the reference angle, then we have

$$y_{\phi,n}^{(1)} = \int_{-\pi}^{\pi} p_\phi^n(\phi) \exp\left[jk\Delta d_{\mathrm{BS}}\left(\phi_0^n - \phi\right)\right] d\phi, \tag{A·1}$$

where

$$p_\phi^n(\phi) = \frac{Q_n \eta_\phi^n}{\sqrt{2}\sigma_\phi^n} \exp\left(-\frac{\sqrt{2}|\phi|}{\sigma_\phi^n}\right). \tag{A·2}$$

For uniformly spaced antennas with separation d_{Tx}, the wave path difference between the uth and u'th antennas, which is introduced by the nth cluster of the PAS at the Tx side, is given by

$$\Delta d_{\mathrm{Tx}}\left(\phi_0^n - \phi\right) = d_{\mathrm{Tx}}\left(u - u'\right) \sin\left(\phi_0^n - \phi\right). \tag{A·3}$$

Expanding $\sin(\phi_0^n - \phi)$ with a first-order Taylor series, we have

$$\begin{aligned} \sin(\phi_0^n - \phi) &= \sin(\phi_0^n)\cos(\phi) - \cos(\phi_0^n)\sin(\phi) \\ &\approx \sin(\phi_0^n) - \phi\cos(\phi_0^n). \end{aligned} \tag{A·4}$$

For brevity, define the following quantities

$$\alpha(\phi_0^n) = kd_{\mathrm{Tx}}(u-u')\sin(\phi_0^n), \quad (\mathrm{A}\cdot 5)$$

$$\beta(\phi_0^n) = kd_{\mathrm{Tx}}(u-u')\cos(\phi_0^n). \quad (\mathrm{A}\cdot 6)$$

Since

$$y_\phi^{(1)} = \sum_{n=1}^{N_C} y_{\phi,n}^{(1)} = \sum_{n=1}^{Nc} \int_{-\pi}^{\pi} p_\phi^n(\phi) \exp\left[jk\Delta d_{\mathrm{Tx}}\left(\phi_0^n - \phi\right)\right] d\phi, \quad (\mathrm{A}\cdot 7)$$

substituting (A· 4), (A· 5) and (A· 6) into (A· 7), we get

$$y_\phi^{(1)} \approx \sum_{n=1}^{N_C} \left\{ \exp[j\alpha(\phi_0^n)] \int_{-\pi}^{\pi} p_\phi^n(\phi) \exp[-j\beta(\phi_0^n)\phi] d\phi \right\} = \sum_{n=1}^{N_C} \left\{ \exp[j\alpha(\phi_0^n)] \mathcal{F}_\omega[p_\phi^n(\phi)] \right\} \Big|_{\omega=\beta(\phi_0^n)}, \quad (\mathrm{A}\cdot 8)$$

where $\mathcal{F}_\omega(\cdot)$ denotes the Fourier transform evaluated at $\omega = \beta(\phi_0^n)$. Using (A· 9) [32], we get (22).

$$\mathcal{F}_\omega\left[\exp\left(-a|x|\right)\right] = \frac{2a}{a^2+\omega^2} \quad (\mathrm{A}\cdot 9)$$

Similarly, $y_\phi^{(2)}$ can be expressed as

$$y_\phi^{(2)} \approx \sum_{n=1}^{N_C} \left\{ \exp[j\alpha(\phi_0^n)] \cdot \int_{-\pi}^{\pi} p_\phi^n(\phi) \cos^2(\phi-\phi_0^n) \exp[-j\beta(\phi_0^n)\phi] d\phi \right\}. \quad (\mathrm{A}\cdot 10)$$

By expanding the trigonometric function in the integral, we get

$$\cos^2(\phi-\phi_0^n) = \frac{1+\cos\left[2\left(\phi-\phi_0^n\right)\right]}{2} = \frac{1+\cos(2\phi)\cos\left(2\phi_0^n\right)+\sin(2\phi)\sin\left(2\phi_0^n\right)}{2}. \quad (\mathrm{A}\cdot 11)$$

Substituting (A· 11) into (A· 10), we have

$$y_\phi^{(2)} = \frac{1}{2}\sum_{n=1}^{N_C} \exp[j\alpha(\phi_0^n)] \Big\{ \mathcal{F}_\omega[p_\phi^n(\phi)] + \cos(2\phi_0^n)\mathcal{F}_\omega[\cos(2\phi)p_\phi^n(\phi)] + \sin(2\phi_0^n)\mathcal{F}_\omega[\sin(2\phi)p_\phi^n(\phi)] \Big\} \Big|_{\omega=\beta(\phi_0^n)}. \quad (\mathrm{A}\cdot 12)$$

Applying (A· 9) and (A· 13) [32], the (A· 12) can be solved. Then, we achieve (24).

$$\mathcal{F}_\omega\left[\exp(-a|x|\cos(bx))\right] = \left[\frac{a}{a^2+(b+\omega)^2} + \frac{a}{a^2+(b-\omega)^2}\right] \quad (\mathrm{A}\cdot 13)$$

The (23) and (25) can be obtained similarly.

Xin Nie received the B.S.E.E. and M.S.E.E. degrees from Beijing University of Aeronautics and Astronautics, Beijing, China, in 2003 and 2006, respectively. He is currently working towards his Ph.D. degree at Beijing University of Posts and Telecommunications (BUPT), Beijing, China. His current research interests include radio propagation, wideband channel measurement, channel parameter estimation and MIMO performance evaluation in real propagation environments.

Jianhua Zhang received the M.S.E.E. and Ph.D. degrees from BUPT, Beijing, China, in 2000 and 2003, respectively, both in circuits and systems. From February 2008 to June 2008, she worked at the Electronics and Telecommunications Research Institute, Korean, as a visiting scholar. She currently is an associate professor of BUPT. Her research interests include transmission techniques of IMT-Advanced systems, broadband MIMO channel measurements and modeling, and cooperative transmission technique.

Ping Zhang received the Ph.D. degree from BUPT, Beijing, China, in 1990 in electronics engineering. He was a Postdoctoral Researcher in the PCS Department, Korea Telecom Wireless System Development Center. Currently, he is a professor of BUPT and director of Wireless Technology Innovation Institute, BUPT. He has also served as the Senior Member of C3G Group, China MOST 863 future mobile communication Fu-TURE project, Vice-Chairman of World Wireless Research Forum (WWRF). Until now, he has published 6 books, around 400 publications in journals and conferences in the area of the key techniques of B3G and 3G systems.